Development of near-infrared fluorescence probe for the selective detection of severe hypoxia

Takafumi Kasai, [†] Kyohhei Fujita, [§] Toru Komatsu, [†] Tasuku Ueno, [†] Ryosuke Kojima, [§] Kenjiro Hanaoka,[#] and Yasuteru Urano[†,§,//]

[†]Graduate School of Pharmaceutical Sciences and [§]Graduate School of Medicine, The University of Tokyo, 7-3-1 Hongo, Bunkyo-ku, Tokyo 113-0033, Japan.

[#]Graduate School of Pharmaceutical Sciences, Keio University, 1-5-30 Shibakoen, Minato-ku, Tokyo 105-8512, Japan.

[//] uranokun@m.u-tokyo.ac.jp

ABSTRACT:

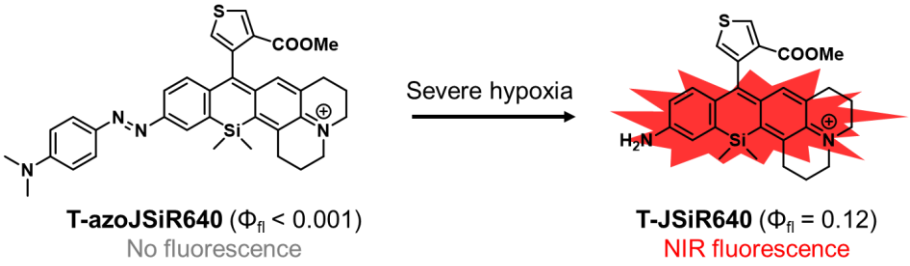

Severely hypoxic environments with oxygen concentrations around 1% are often found in serious diseases such as ischemia and cancer. However, existing near-infrared (NIR) fluorescence probes that can visualize hypoxia are also activated in mildly hypoxic environments (around 5% oxygen). Here, in order to selectively detect severe hypoxia, we used julolidine-based SiR (JSiR) as a NIR fluorophore and developed T-azoJSiR640 as a fluorescence probe. T-azoJSiR640 was able to detect severe hypoxia (around 1% oxygen concentration or less) in live cell imaging. Furthermore, the ischemic liver in a portal-vein-ligated mouse model was successfully visualized *in vivo*.

■ INTRODUCTION

Hypoxia, generally considered as an oxygen concentration of <2%,[1] is found in various diseases such as ischemia,[2,3] chronic kidney disease[4,5] and cancer.[6–9] Indeed, oxygen concentrations as low as around 1% may occur in ischemia[10–12] and cancer,[13,14] and selective *in vivo* visualization of such severe hypoxia is especially important for monitoring and understanding these diseases. To analyze hypoxia *in cellulo* and *in vivo*, various fluorescence probes have been developed.[15–19] However, existing near-infrared (NIR) small molecular probes that can be effectively used *in vivo* are also activated at oxygen concentrations around 5%.[15,19–21] Therefore, there is a need for the development of NIR fluorescence probes able to selectively detect severe hypoxia as *in vivo* analytical and diagnostic tools.

Our research group has focused on the reductive cleavage of azo groups under hypoxia and developed NIR probes based on fluorescence resonance energy transfer (FRET) between dicarbocyanines and Black Hole Quencher (BHQ).[22] Although these probes are selectively activated in severe hypoxia, they are not optimal for *in cellulo* and *in vivo* applications due to their large molecular size and susceptibility to photobleaching. As another strategy, we have recently developed fluorescence probes that detect hypoxia by incorporating an azo group into an O rhodamine or Si rhodamine (SiR) scaffold.[21,23] For example, we have developed green-emitting MAR,[23] red-emitting MASR[23] and NIR-emitting azoSiR640 (2,6-diMe azoSiR640),[21] and confirmed that they can detect hypoxia in cultured cells and mouse models. These fluorescence probes initially have no fluorescence due to fluorescence quenching by the azobenzene moiety incorporated in the fluorophore. Upon cleavage of the azo group by reductase-catalyzed reactions that are accelerated in hypoxia, corresponding fluorescent rhodamines are produced, enabling selective detection of hypoxia. However, the oxygen concentration threshold of these rhodamine-based hypoxia probes varies depending on the fluorescent scaffold. For example, MASR and 2,6-diMe azoSiR640 switched on at around 0.1% and 5% oxygen concentration, respectively.[21,23] These characteristics may be due to differences in the rate of reverse oxidation of the azo moiety depending on the fluorescent scaffold (**Figure S1**). Thus, we considered that the development of NIR probes to selectively detect severe hypoxia of around 1% oxygen concentration might be achieved by using different fluorophores.

The mono-julolidine-fused analog of SiR (JSiR) is widely used as a NIR fluorophore for biological imaging.[24] In this study, we therefore examined JSiR as the scaffold fluorophore of a NIR fluorescence probe for hypoxia. We also evaluated the responsiveness of the synthesized probe, T-azoJSiR640, to oxygen concentration and confirmed its utility to selectively detect severe hypoxia *in vivo*.

■ RESULTS AND DISCUSSION

Design and synthesis of compounds. Since the oxygen concentration threshold of rhodamine-based hypoxia probe varies depending on the scaffold fluorophore,[21,23] we focused here on JSiR as a widely used NIR fluorophore with different redox behavior from other SiR fluorophores. Building on our previously reported MASR[23] and 2,6-diMe azoSiR640,[21] we designed and developed a novel fluorescence probe for hypoxia by introducing an azobenzene moiety at a free amino group of JSiR (**Figure 1**). Since bulky substitutions at the 2nd or 6th positions of the benzene ring in SiR block nucleophilic attack at the 9th position of the xanthene ring,[21,25,26] for example, by water and cysteine containing molecules, we firstly designed a probe possessing carboxylic acid at the 2nd position of the benzene ring of JSiR. However, this proved synthetically difficult, requiring tedious synthetic and purification steps. So, we next designed a probe possessing a thiophene ring instead of the benzene ring. We synthesized this probe, Tc-azoJSiR640, as shown in **Scheme 1**, but it proved ineffective due to its poor cellular membrane permeability (**Figure S2**). Since the reason for this was considered to be the presence of the anionic form of the carboxylic acid moiety,[27–29] we converted it to a methoxycarbonyl group and synthesized T-azoJSiR640. Compared to Tc-azoJSiR640, the membrane permeability of T-azoJSiR640 was apparently improved, as described later. Therefore, we focused on T-azoJSiR640 and evaluated its optical properties and susceptibility to hypoxia.

Optical properties and stability of developed probes. We next evaluated the optical properties of synthesized T-azoJSiR640 and T-JSiR640 (**Table 1**). T-JSiR640 was expected to be produced from T-azoJSiR640 under reductive conditions (hypoxia) (**Figure 2(a)**). T-azoJSiR640 showed a broad absorbance spectrum with no fluorescence in sodium phosphate buffer (100 mM; pH 7.4) (**Figures 2(b, c)**). The observed complete quenching of fluorescence was considered to be due to ultrafast cis/trans conformational change of the azo bond of T-azoJSiR640 in the excited state, as in the case of our previously reported probes. [21–23] On the other hand, T-JSiR640 showed marked fluorescence with a peak at 662 nm in the NIR range (**Figure 2 (c)**), and its fluorescence quantum yield was 0.12 (**Table 1**). We also confirmed that T-JSiR640 showed essentially the same fluorescence spectra over the pH range from 5.0 to 9.0, indicating that fluorescence signal of T-JSiR640 is not affected by pH (**Figure S3**). These results suggested that T-azoJSiR640 is able to generate NIR fluorescence upon cleavage of the azo group under hypoxia.

Rat liver microsome assay. To determine whether T-azoJSiR640 could detect hypoxia, we first performed an *in vitro* assay using rat liver microsomes, which contain various reductases such as NADPH-cytochrome P450 reductase. The probe T-azoJSiR640 showed a fluorescence increase only in the presence of rat liver microsomes and NADPH under hypoxia, indicating that the probe could detect hypoxia under reducing conditions catalyzed by microsomal reductases (**Figure 2(d)**).

Live cell fluorescence imaging of hypoxia. To evaluate whether T-azoJSiR640 could visualize hypoxia in living cells, we used it to perform live-cell fluorescence imaging of A549 lung

adenocarcinoma cells under various oxygen concentrations. T-azoJSiR640 showed almost no fluorescence under normoxia (**Figures 3(a, b)**), while it showed significant increase of NIR fluorescence at oxygen concentration around 1%. These results suggested that T-azoJSiR640 was able to selectively detect severe hypoxia. [17] In contrast with the above results, our previously reported 2,6-diMe azoSiR640 was also activated at around 5% oxygen concentration (**Figures 3(a, b)**). To confirm that the observed fluorescence signals were due to reduction by flavoproteins, we measured fluorescence images in the presence of a NADPH oxidase inhibitor, diphenyleneiodonium chloride (DPI). [30] The fluorescence increase was dramatically suppressed in the presence of DPI, suggesting that T-azoJSiR640 is reduced by flavoproteins such as NADPH-cytochrome P450 reductase.

We assumed that this selective activation of T-azoJSiR640 around 1% oxygen concentration is due to the high rate of reverse oxidation of the azo anion radical produced in the first reduction step (**Figure S1**). This would explain why the fluorescence signal of T-azoJSiR640 is suppressed around 20-3% oxygen concentration, but is activated in extremely low oxygen concentration (around 1%), thereby allowing the selective detection of severe hypoxia.

***In vivo* fluorescence imaging of liver ischemia in mouse models.** Finally, we performed fluorescence imaging of liver ischemia of mouse to determine whether T-azoJSiR640 could detect severe hypoxia *in vivo*. The probe T-azoJSiR640 was administered to mice by intravenous injection, and after 30 min, the portal vein was ligated to induce ischemia. Before ligation of the portal vein, no fluorescence increase was observed in the liver, while a rapid and significant fluorescence increase was observed over the entire liver after the induction of ischemia (**Figures 3(c, d)**). To confirm that T-JSiR640 was produced, we examined the production of T-JSiR640 by LC-MS/MS analysis (**Figures S5**). Indeed, T-JSiR640 was selectively generated in liver ischemia, while it was not detected in the liver of mice without portal vein ligation (**Figures S4 and S5**), indicating that T-azoJSiR640 was selectively activated in ischemic tissues. These results demonstrated that T-azoJSiR640 can visualize severe hypoxia *in vivo*.

■ CONCLUSIONS

We have designed, synthesized, and evaluated T-azoJSiR640 as a NIR fluorescence probe for severe hypoxia. In contrast to existing NIR probes for hypoxia, T-azoJSiR640 was able to selectively visualize severe hypoxia (around 1% oxygen concentration or less) in live cells and in ischemic liver of a mouse model *in vivo*. Our results demonstrated that the developed NIR fluorescence probe T-azoJSiR640 has the potential to be useful tool for analyzing, monitoring and understanding various hypoxia-related diseases.

■ EXPERIMENTAL PROCEDURES

Abbreviations. AcOEt, ethyl acetate; AcOH, acetic acid; Ar, argon; CH_2Cl_2, dichloromethane; DMEM, Dulbecco's modified Eagle's medium; DMF, *N,N*-dimethylformamide; DMSO, dimethyl sulfoxide; DPI, diphenyleneiodonium chloride; ESI, electrospray ionization; ε, molar extinction coefficient; FBS, fetal bovine serum; Φ_{fl}, fluorescence quantum efficiency; H_2O, water; HPLC, high-performance liquid chromatography; KCl, potassium chloride; K_2CO_3, potassium carbonate; LC/MS, liquid chromatography mass spectrometry; MeCN, acetonitrile; MeOH, methanol; NADPH, nicotinamide adenine dinucleotide phosphate; $NaHCO_3$, sodium hydrogen carbonate; NMR, nuclear magnetic resonance; Na_2SO_4, sodium sulfate; $Na_2S_2O_3$, sodium thiosulfate; PBS, phosphate-buffered saline; PS, penicillin-streptomycin; TCL, thin layer chromatography; TFA, trifluoroacetic acid; THF, tetrahydrofuran.

General Procedures and Materials. Reagents and solvents were of the best grade available, purchased from Tokyo Chemical Industries, Wako Pure Chemical, Aldrich Chemical Co., Dojindo, and Invitrogen, and were used without further purification. Reactions were monitored by means of TLC, ESI mass spectrometry and HPLC. All compounds were purified by silica gel chromatography or preparative HPLC.

Characterization of compounds. NMR spectra were recorded on a JNM-ECZ400S instrument at 400 MHz for ^{1}H NMR and at 100 MHz for ^{13}C NMR. Mass spectra were measured with a JEOL JMS-T100LP mass spectrometer (ESI^+).

Preparative HPLC methods. Preparative HPLC was performed on an Inertsil ODS-3 5 μm (10.0 × 250 mm) column (GL Sciences, Tokyo, Japan) using an HPLC system composed of a pump (PU-2086, JASCO) and a detector (MD-2015 or FP-2025, JASCO). Eluent A (H_2O containing 0.1% TFA), eluent B (80% MeCN and 20% H_2O containing 0.1% TFA), eluent C (H_2O containing 10 mM ammonium formate), eluent D (MeCN containing 0.1% TFA) and eluent E (MeCN containing 10 mM ammonium formate) were used for HPLC purification.

HPLC analysis for reaction monitoring. HPLC analysis were performed on a Waters Acquity UPLC (H class)/QDa quadrupole MS analyzer or Acquity UPLC (H class)/xevo TQD quadrupole MS/MS analyzer equipped with an Acquity UPLC BEH C18 1.7 μm (2.1×50 mm) column (Waters). Eluent C and eluent E, or eluent F (H_2O containing 0.1% formic acid) and eluent G (MeCN containing 0.1% formic acid) were used.

Optical Properties and Fluorescence Quantum Efficiency. Fluorescence spectra were obtained with a Hitachi F-7000 or F-7100. The slit width was 5 nm for both excitation and emission. The photomultiplier voltage was 700 V. UV-visible absorption spectra were obtained with a Shimadzu UV-1850 or UV-2450. Fluorescence quantum efficiency was measured with a Quantaurus-QY (Hamamatsu Photonics) in 100 mM potassium phosphate buffer at pH 7.4.

Probe stock solution. T-azoJSiR640 was weighed, dissolved in methanol and aliquoted to 1.5

mL Microtube Black for Shading (WATSON® BIO LAB). The solvent was evaporated and the tubes were stored at -25˚C. The samples were reinstated in an appropriate solvent before use. The probe solution was prepared individually for each experiment and not reused. T-JSiR640 was solved in DMSO and stored in Safe-Lock Tubes 1.5 mL at -25°C. The concentrations of stock solutions were calculated from the by ε values.

Preparation of rat liver microsomes. All animal experiments were performed according to institutional guidelines. Rats (Wistar, boar, 6-7 weeks old at the beginning of the experiment) were purchased from CLEA Japan. They were treated with 60 mg/5 mL/kg sodium phenobarbital intraperitoneally once daily for 3 days, fasted overnight, and sacrificed by exsanguination from the abdominal aorta. The livers containing 0.15 M KCl at pH 7.4 were homogenized in 3 equal volumes of the same buffer and centrifuged (8,500 rpm, 20 min, 4°C) twice. Then the supernatant was collected and centrifuged (34,000 rpm, 80 min, 4°C) to collect rat liver microsomal fractions. Rat liver microsomes contained 71.2 mg protein/mL and 0.479 nmol P450/mg protein. The microsome fraction was diluted in 100 mM sodium phosphate buffer at pH 7.4 for assay.

Rat liver microsome assay. The *in vitro* hypoxic environment was prepared in a sealed cuvette. The assay solution (2 mL of 100 mM potassium phosphate buffer at pH 7.4) containing 3 μM T-azoJSiR640, rat liver microsomes (76 μg/mL) and 0.1% MeOH was bubbled with Ar gas for 30 min. As a reductase cofactor, 128 μM NADPH was added at 240 sec, and fluorescence intensity was measured over 7000 sec at 37˚C.

Cell lines and culture conditions. A549 lung adenocarcinoma cells were purchased from the RIKEN BioResource Center Cell Bank. A549 cells were cultured in DMEM containing 10% FBS and 1% PS at 37˚C under 5% CO_2 air.

Live cell fluorescence imaging of hypoxia. A549 (3.0×10^4 cells, passage>3) were seeded on 8-chamber plates (NIPPON Genetic Co., Ltd.) and cultured for 1 day before assay. On the next day, DMEM was removed and 200 μL phenyl red (-) DMEM supplemented with 10% FBS and 1% PS containing 1 μM probe and 1% DMSO as a co-solvent was added. The cells were incubated for 6 h under various oxygen concentrations (0.3, 1, 3, 20%) and 5% CO_2 at 37˚C (**Figures 2(a) and 2S (a)**). The oxygen concentrations was controlled with a multi gas incubator MCO-5MUV (Sanyo) by N_2 substitution. Fluorescence confocal microscopy images were acquired using a Leica Application Suite Advanced Fluorescence (LAS-AF) instrument equipped with a TCS SP5 and 40× or 10× objective lens. Gain and pinhole values were set at 150% and 95.0 μm (**Figures 2(a)**) or 68.0 μm (**Figure S2(a)**). The light source was a white light laser. The excitation and emission wavelengths were 630 nm/ 650-750 nm. The inhibitor experiment was performed by adding 30 μM DPI. The fluorescence intensity of the entire image area was quantified by Image-J.

***In vivo* fluorescence imaging of liver ischemia in mouse models.** All procedures were approved by the Animal Care and Use Committee of the University of Tokyo. Female Jcl: ICR mice

(7 weeks) were used. T-azoJSiR640 (200 μM) in PBS (150 μL) containing 4% ethanol was administered by intravenous injection. After probe administration, the mice were anesthetized with a combination of domitor, butorphanol and midazolam. Fluorescence images were captured at 10 min, 20 min and 30 min after administration of the probe, and then the portal vein was ligated with suture thread at 30 min. Further fluorescence images were captured at 40 min, 50 min and 60 min. All fluorescence images were captured with the CRi Maestro imaging system (CRi Inc., Woburn, MA). Exposure time was 70 msec. The stage was set at 1B. The emission filter was Longpass Filter / VIS 650 nm (Asahi Spectra Co., Ltd.) and the excitation filter was Bandpass Filter / 600 nm (Asahi Spectra Co., Ltd.).

LC-MS/MS analysis of resected liver. LC-MS/MS analysis was performed using the LC system Acquity UPLC H-Class (Waters) equipped with an Acquity UPLC BEH C18 1.7 μm (2.1×50 mm) column (Waters) and an MS/MS detector (Xevo TQD, Waters). Eluent F (H_2O containing 0.1% formic acid) and eluent H (80% MeCN and 20% H_2O containing 0.1% formic acid) were used with the following binary linear gradient conditions: F/H = 95/5 isocratic for 0.3 min, then linearly shifted to 5/95 over 2.7 min. Flow rate was 0.8 mL/min. MS detection was in the positive ion mode with multiple reaction monitoring (MRM) settings. The frozen liver sections (50-100 mg) were extracted with 10 volumes of 80% MeCN and 20% H_2O containing fluorescein (1 μM) as an internal standard. The extract was centrifuged (14,000 rpm, 10 min, 4°C), and the supernatant was collected and stored at 0°C before analysis. 5 mL of sample was used for the analysis, and the expected concentrations were calculated from calibration curve prepared by independently injecting T-JSiR640 and T-azoJSiR640. For MRM analysis, *m/z* = 59.1 > 473.2, 89.0 > 473.2 (cone voltage = 50 V, collision energy = 90 V) was monitored for T-JSiR640, and *m/z* = 89.0 > 605.2, 120.1 > 605.2, 456.2 >605.2 (cone voltage = 30 V, collision energy = 90 V) was monitored for T-azoJSiR640.

AUTHOR INFORMATION

Corresponding Author

*E-mail: uranokun@m.u-tokyo.ac.jp.

Notes

The authors declare no competing financial interest.

■ ACKNOWLEDGMENTS

This research was supported in part by AMED under grant number JP19gm0710008 (to Y.U.), by MEXT/JSPS KAKENHI grants JP16H02606, JP26111012, and JP19H05632 (to Y.U.). JSPS KAKENHI grant number 22K20528, JST, ACT-X grant number JPMJAX222G and Masason Foundation (to K.F.), MEXT/JSPS KAKENHI grants JP21H05262 (to K.H.) and World-leading INnovative Graduate Study Program for Life Science and Technology (WINGS-LST) (to Takafumi.K.).

Scheme, figure and table legends

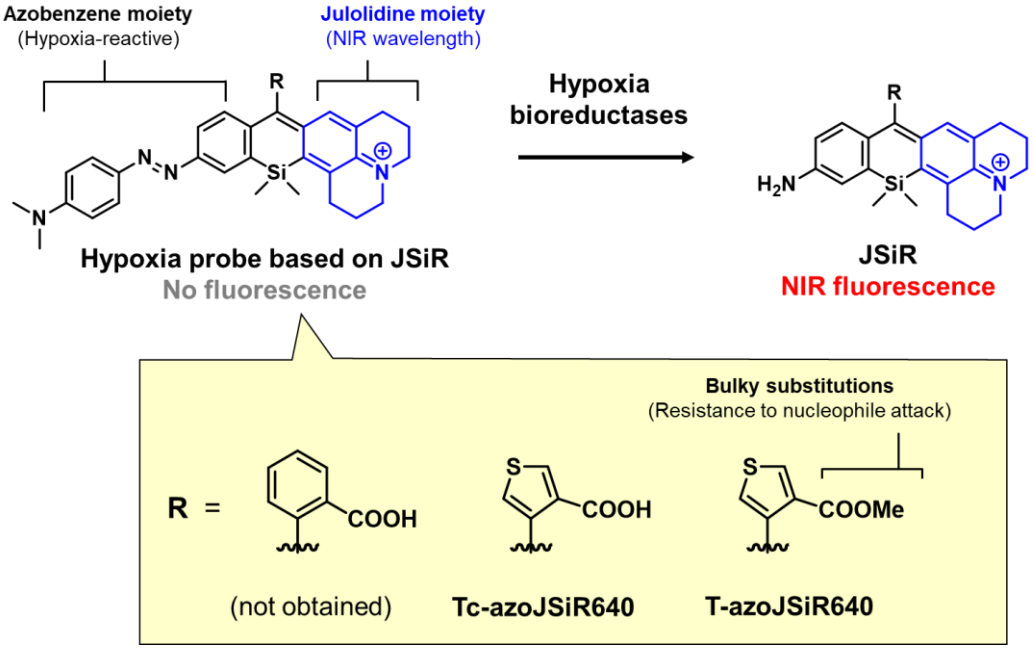

Figure 1. Molecular design of NIR fluorescence probe for hypoxia based on JSiR.

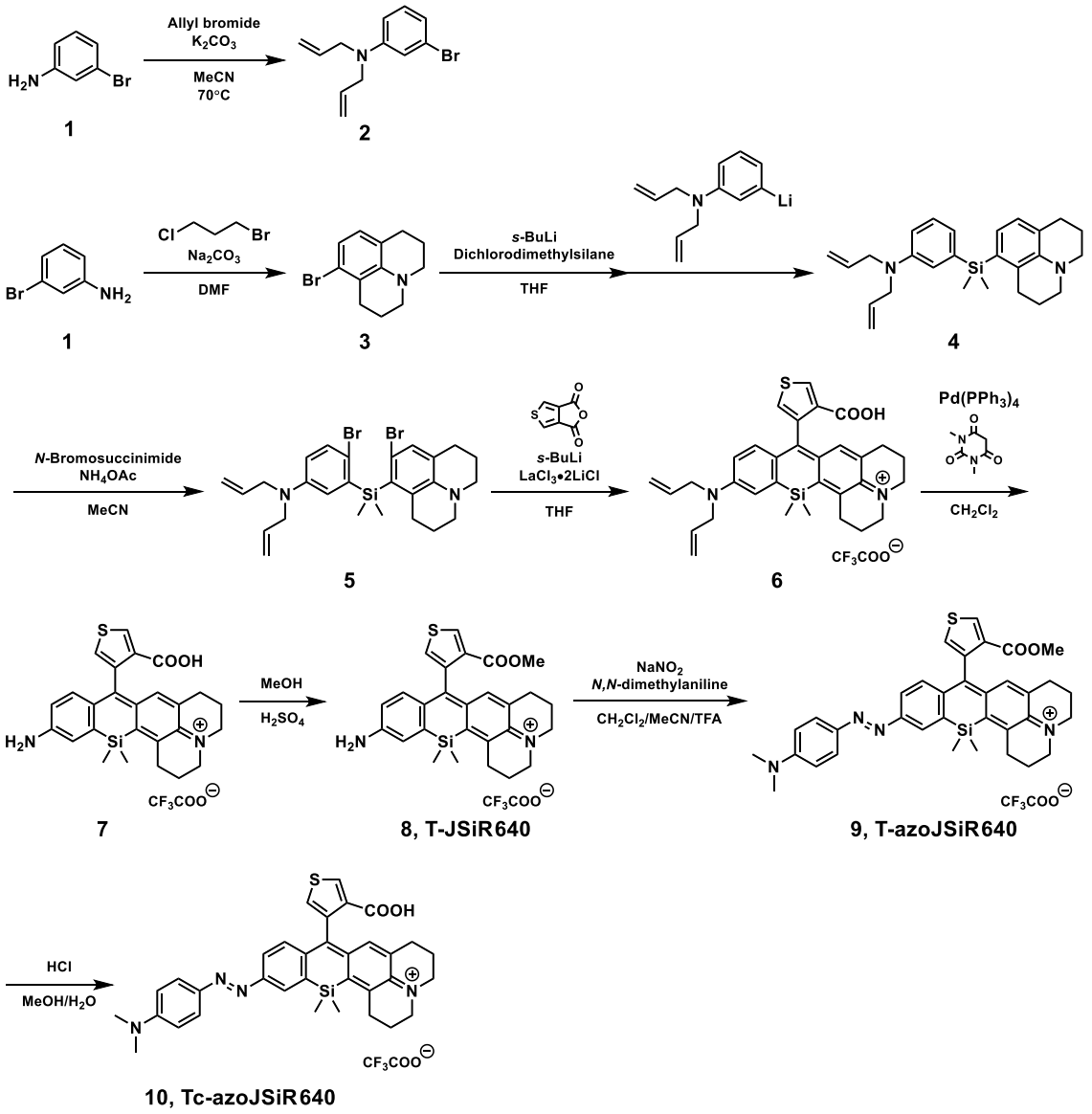

Scheme 1. Synthetic scheme of T-azoJSiR640 and Tc-azoJSiR640.

Table 1. Photophysical properties of T-azoJSiR640 and T-JSiR640 in sodium phosphate buffer at pH 7.4.

	λ_{abs} [nm]	λ_{fl} [nm]	Φ_{fl}
T-azoJSiR640	597	n.d.	<0.001
T-JSiR640	641	662	0.12

n.d. = not detectable

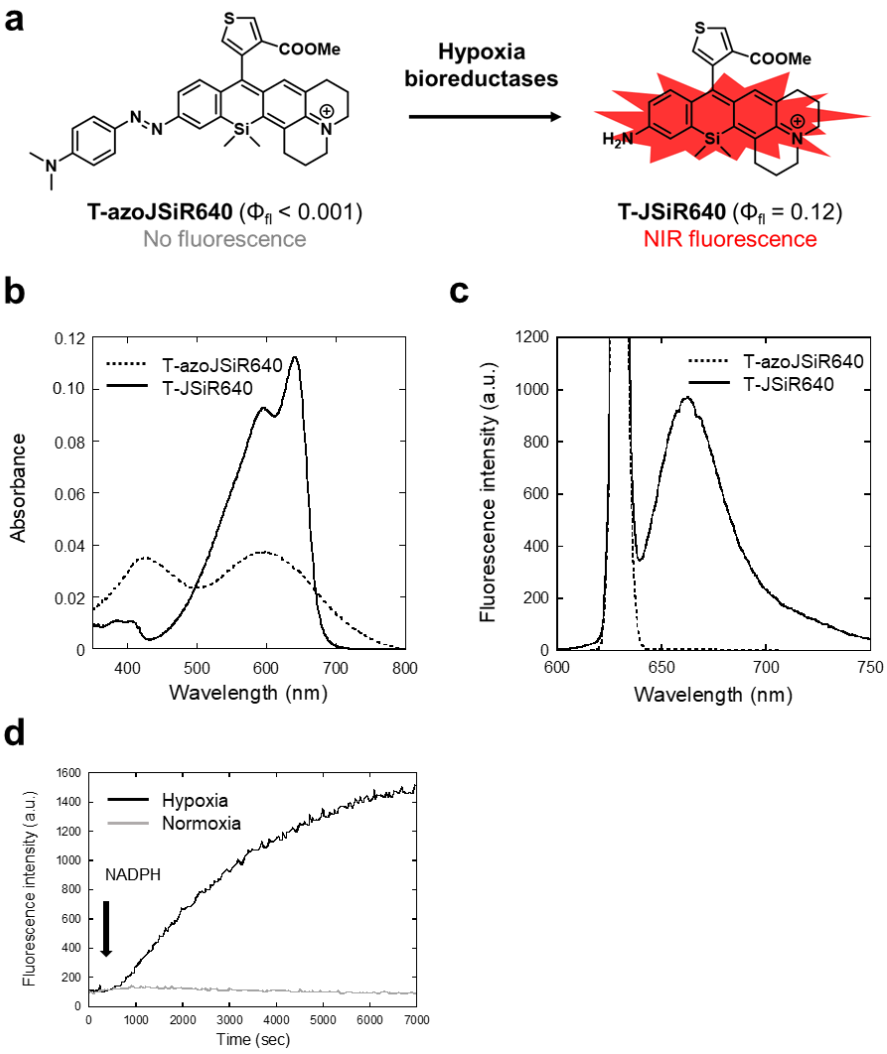

Figure 2. Developed NIR fluorescence probe for hypoxia, T-azoJSiR640. (a) NIR fluorescence activation of T-azoJSiR640. T-azoJSiR640 is non fluorescent, but is converted to fluorescent T-JSiR640 by bio-reductases under hypoxia. **(b)** Absorbance spectra of T-azoJSiR640 and T-JSiR640. [T-azoJSiR640] = 1.0 μM, [T-JSiR640] =1.0 μM. Both spectra were measured in 100 mM sodium phosphate buffer at pH 7.4 including 0.1% MeOH or 0.1% DMSO, respectively. **(c)** Fluorescence spectra of T-azoJSiR640 and T-JSiR640. [T-azoJSiR640] = 0.3 μM, [T-JSiR640] = 0.3 μM. Both spectra were measured in 100 mM sodium phosphate buffer at pH 7.4 including 0.1% MeOH or 0.1% DMSO, respectively. **(d)** Time-dependent fluorescence changes of T-azoJSiR640 in the presence of rat liver microsomes under hypoxia and normoxia at 37°C. Assays were performed in 100 mM sodium phosphate buffer at pH 7.4 containing 0.5% MeOH as a cosolvent. The hypoxic environment was prepared by bubbling Ar gas for 30 min. NADPH was added at 4 min. The excitation and emission

wavelengths were 630 nm and 650 nm. [T-azoJSiR640] = 3.0 μM, [rat liver microsomes] = 76 μg/mL, [NADPH] = 128 μM.

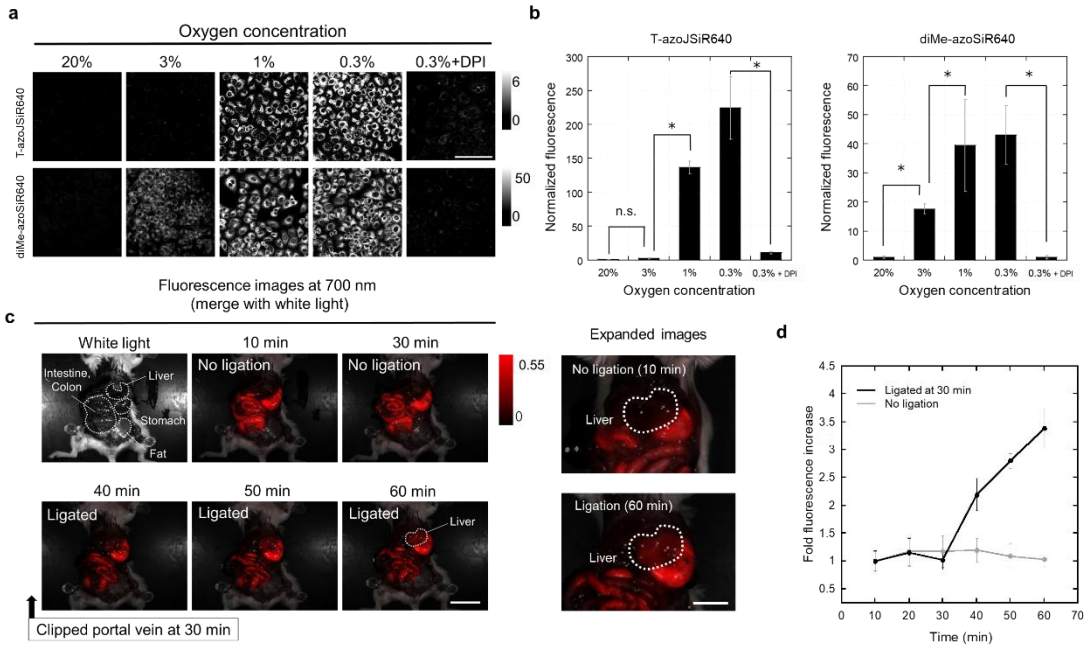

Figure 3. Live cell and *in vivo* fluorescence imaging of hypoxia. (a) Fluorescence images of A549 cells incubated with T-azoJSiR640 and 2,6-diMe azoSiR640 under various oxygen concentrations (20%, 3%, 1% and 0.3%). The inhibitor experiment was performed by the addition of the probe and DPI under 0.3% oxygen concentration. All fluorescence images were captured 6 h after administration of the probe. Fluorescence imaging was performed in phenol red (-) DMEM containing 10% FBS, 1% PS and 1% DMSO as a cosolvent. The excitation and emission wavelengths were 630 nm/650-750 nm. [probe] = 1 μM. [DPI] = 30 μM. Scale bars = 100 μm. **(b)** Comparison of fluorescence intensities at each oxygen concentration (n = 4). Fluorescence intensity of individual condition was normalized to that of 20% oxygen concentration. $*p < 0.05$ by Student's *t*-test. Error bar represents S.D. **(c)** *In vivo* fluorescence imaging of liver ischemia of mouse models. 200 μM T-azoJSiR640 in PBS (150 μL) containing 4% ethanol (*v*/*v*) as a cosolvent was administered by intravenous injection. The portal vein was ligated with thread at 30 min after probe injection to induce liver ischemia. The liver showed an NIR fluorescence increase only after induction of ischemia. The excitation and emission wavelengths were 570-630 nm/650- nm. Scale bars = 2 cm (left) or 1 cm (right). **(d)** Fold fluorescence increase of liver at 700 nm (n = 3). Fold fluorescence increase represents increase at 10 min after administration of the probe. Ischemic liver showed a specific fluorescence increase. $*p < 0.05$ by Student's *t*-test. Error bar represents S.D.

■ REFERENCES

1. Chen, P. S. *et al*. (2020) Pathophysiological implications of hypoxia in human diseases. *J. Biomed. Sci.*, **27**, 63.
2. Adhami, F. *et al*. (2006) Cerebral Ischemia-Hypoxia Induces Intravascular Coagulation and Autophagy. *Am. J. Pathol.*, **169**, 566–583.
3. Baron, J.-C. (2001) Perfusion Thresholds in Human Cerebral Ischemia: Historical Perspective and Therapeutic Implications. *Cerebrovasc. Dis*., **11**, 2-8.
4. Hirakawa, Y., Tanaka, T. & Nangaku, M. (2017) Renal hypoxia in CKD; Pathophysiology and detecting methods. *Front. Psychol.*, **8**:99.
5. Nangaku, M. (2006) Chronic hypoxia and tubulointerstitial injury: A final common pathway to end-stage renal failure. *J. Am. Soc. Nephrol.*, **17**, 17–25.
6. Wilson, W. R. & Hay, M. P. (2011) Targeting hypoxia in cancer therapy. *Nat. Rev. Clin. Oncol.*, **11**, 393–410.
7. Melillo, G. (2007) Targeting hypoxia cell signaling for cancer therapy. *Cancer Metastasis Rev*., **26**, 341–352.
8. Poon, E., Harris, A. L. & Ashcroft, M. (2009) Targeting the hypoxia-inducible factor (HIF) pathway in cancer. *Expert Rev. Mol. Med.*, **11**, E26.
9. Zhang, Y., Coleman, M. & Brekken, R. A. (2021) Perspectives on hypoxia signaling in tumor stroma. *Cancers*, **13**, 3070.
10. Valadka, A. B. *et al*. (1998) Relationship of brain tissue PO_2 to outcome after severe head injury. *Crit. Care Med.*, **26**, 1576-1581.
11. Sekhon, M. S. *et al*. (2020) Brain Hypoxia Secondary to Diffusion Limitation in Hypoxic Ischemic Brain Injury Postcardiac Arrest. *Crit. Care Med.*, **48**, 378–384.
12. van den Brink, W. A. *et al*. (2000) Brain Oxygen Tension in Severe Head Injury. *Neurosurgery*., **46**, 868-878.
13. Muz, B., de la Puente, P., Azab, F. & Azab, A. K. (2015) The role of hypoxia in cancer progression, angiogenesis, metastasis, and resistance to therapy. *Hypoxia*., **3**, 83-92.
14. Vaupel, P. & Mayer, A. (2007) Hypoxia in cancer: Significance and impact on clinical outcome. *Cancer Metastasis Rev.*, **26**, 225–239.
15. Cui, L. *et al*. (2017) A NIR turn-on fluorescent probe applied in cytochrome P450 reductase detection and hypoxia imaging in tumor cells. *Dyes Pigm.*, **139**, 587–592.
16. Wang, S. *et al*. (2023) A highly sensitive NIR fluorescence probe for hypoxia imaging in cells and ulcerative colitis. *Talanta*, **252**.
17. Kumari, R. *et al*. (2021) A Nitronaphthalimide Probe for Fluorescence Imaging of Hypoxia in Cancer Cells. *J. Fluoresc*., **31**,1665–1673.
18. Tian, Y. *et al*. (2020) Novel Strategy for Validating the Existence and Mechanism of the ‘gut-Liver

Axis' in Vivo by a Hypoxia-Sensitive NIR Fluorescent Probe. *J. Anal. Chem*., **92**, 4244–4250.

19. Guo, T. *et al*. (2013) A highly sensitive long-wavelength fluorescence probe for nitroreductase and hypoxia: Selective detection and quantification. *Chem. Commun.*, **49**, 10820–10822.
20. Fukuda, S. *et al*. (2016) In vivo retinal and choroidal hypoxia imaging using a novel activatable hypoxia-selective near-infrared fluorescent probe. *Graefe's Arch Clin. Exp. Ophthalmol.*, **254**, 2373–2385.
21. Hanaoka, K. *et al*. (2018) Synthesis of unsymmetrical Si-rhodamine fluorophores and application to a far-red to near-infrared fluorescence probe for hypoxia. *Chem. Commun.*, **54**, 6939–6942.
22. Kiyose, K. *et al*. (2010) Hypoxia-sensitive fluorescent probes for in vivo real-time fluorescence imaging of acute ischemia. *J. Am. Chem. Soc.*, **132**, 15846–15848.
23. Piao, W. *et al*. (2013) Development of Azo-Based Fluorescent Probes to Detect Different Levels of Hypoxia. *Angew. Chem. Int. Ed.*, **52**, 13028–13032.
24. Iwatate, R. J. *et al*. (2018) Silicon Rhodamine-Based Near-Infrared Fluorescent Probe for γ-Glutamyltransferase. *Bioconjug. Chem*., **29**, 241–244.
25. Song, Y. *et al*. (2020) Improving Brightness and Stability of Si-Rhodamine for Super-Resolution Imaging of Mitochondria in Living Cells. *Anal. Chem.*, **92**, 12137–12144.
26. Umezawa, K., Yoshida, M., Kamiya, M., Yamasoba, T. & Urano, Y. (2017) Rational design of reversible fluorescent probes for live-cell imaging and quantification of fast glutathione dynamics. *Nat. Chem*., **9**, 279–286.
27. Wang, L., Frei, M. S., Salim, A. & Johnsson, K. (2019) Small-Molecule Fluorescent Probes for Live-Cell Super-Resolution Microscopy. *J. Am. Chem. Soc.*,**141**, 2770–2781.
28. Lavis, L. D. & Raines, R. T. (2014) Bright building blocks for chemical biology. *ACS Chem. Biol.*, **9**, 855–866.
29. Lukinavičius, G. *et al*. (2013) A near-infrared fluorophore for live-cell super-resolution microscopy of cellular proteins. *Nat. Chem.*, **5**, 132–139
30. Chakraborty, S. & Massey, V. (2002) Reaction of reduced flavins and flavoproteins with diphenyliodonium chloride. *J. Biol. Chem.*, **277**, 41507–41516.